

**Evaluations of an ocean bottom electro-magnetometer and preliminary results offshore NE  
Taiwan**

**Ching-Ren Lin<sup>1</sup>, Chih-Wen Chiang<sup>2</sup>, Kuei-Yi Huang<sup>2</sup>, Yu-Hung Hsiao<sup>3</sup>, Po-Chi Chen<sup>3</sup>,  
Hsu-Kuang Chang<sup>3</sup>, Jia-Pu Jang<sup>3</sup>, Kun-Hui Chang<sup>1</sup>, Feng-Sheng Lin<sup>1</sup>, Saulwood Lin<sup>4</sup>, and  
Ban-Yuan Kuo<sup>1</sup>**

1 Institute of Earth Sciences, Academia Sinica, Taipei 11529, Taiwan, R.O.C

2 Institute of Earth Sciences, National Taiwan Ocean University, Keelung 20224, Taiwan, ROC.

3 Taiwan Ocean Research Institute, National Applied Research Laboratories, Kaohsiung 80143,  
Taiwan, R.O.C.

4 Institute of Oceanography, National Taiwan University, Taipei 10617, Taiwan, R.O.C

Corresponding author: Chih-Wen Chiang

Address: Institute of Earth Sciences, National Taiwan Ocean University, Keelung 20224, Taiwan

E-mail: [zjiang@ntou.edu.tw](mailto:zjiang@ntou.edu.tw)

Tel: +886-2-24622192 Ext.6513

Fax: +886-2-24625038

August, 2019

## ABSTRACT

The first stage of field experiments involving the design and construction of a low-power consumption ocean bottom electro-magnetometer (OBEM) has been completed, which can be deployed more than 180 days on the seafloor with time drift less than 0.95 ppm. To improve the performance of the OBEM, we rigorously evaluated each of its units, e.g., the data loggers, acoustic parts, internal wirings, and magnetic and electric sensors, to eliminate unwanted events such as unrecovered or incomplete data. The first offshore deployment of the OBEM together with ocean bottom seismographs (OBSs) was performed in NE Taiwan, where the water depth is approximately 1,400 m. The total intensity of the magnetic field (TMF) measured by the OBEM varied in the range of 44,100–44,150 nT, which corresponded to the proton magnetometer measurements. The daily variations of the magnetic field were recorded using the two horizontal components of the OBEM magnetic sensor. We found that the inclinations and magnetic data of the OBEM varied with two observed earthquakes when compared to the OBS data. The potential fields of the OBEM were slightly, but not obviously, affected by the earthquakes.

**Keywords:** OBEM; data logger; acoustic transceiver; fluxgate; non-polarizing electrodes.

## 1. Introduction

Marine electromagnetic exploration is a geophysical prospecting technique used to reveal the electrical resistivity features of the oceanic upper mantle down to depths of several hundreds of kilometers in different geologic and tectonic environments, such as in areas around mid-oceanic ridges, areas around hot-spot volcanoes, subduction zones, and normal ocean areas between mid-oceanic ridges and subduction zones (Ellis et al., 2008; Evans et al., 2005; Key, 2012; Utada, 2015).

Even though many magnetotelluric explorations have investigated deep electrical structures on Taiwan (Bertrand et al., 2009; Bertrand et al., 2012; Chiang et al., 2011; Chiang et al., 2010; Chiang et al., 2015; Chiang et al., 2008), there were no marine electromagnetic experiments around Taiwan until 2010. The first generation of ocean bottom seismographs (OBSs) was developed by the Institute of Earth Sciences,

Academia Sinica (IES), Taiwan Ocean Institute, National Applied Research Laboratories, and the Institute of Undersea Technology, National Sun Yat-sen University (OBS R&D team), in 2009, the so-called Yardbird-20s. These OBSs have acquired large amounts of data via a series of deployments offshore Taiwan that can be used to study plate tectonics and crustal characteristics (Kuo et al., 2015; Kuo et al., 2012; Kuo et al., 2014). Subsequently, the OBS R&D team developed an ocean bottom electro-magnetometer (OBEM) modified from the OBS based on important developmental experiments.

The novel OBEM was constructed by the OBS R&D team and has completed the first stage of field experiments by the Institute of Earth Sciences, National Ocean Taiwan University, and IES. One OBEM and six broadband OBSs, so-called BBYBs (Broadband Yardbirds), were deployed at the western end of the Okinawa Trough (OT), NE Taiwan, for field testing in March 2018. The water depth in this area is approximately 1,400 m. All the instruments were successfully recovered in May 2018 after collecting the first OBEM field data in Taiwan. Here, we introduce the OBEM design, specifications, calibration procedures, and its further developments and improvements.

## **2. The OBEM design**

The OBEM is designed to be wireless deep-underwater equipment; however, the power supply is limited for the wireless OBEM because the batteries cannot be directly charged via electric cables from vessels. Therefore, designing low-power consumption for the OBEM and high-efficiency battery packs is critically required for long periods of operation. The major units of the OBEM include a data logger, a magnetic sensor, a tiltmeter, electric receivers with an arm-folding mechanism, a relocation system, recovery units, and an anchor. All the units for the OBEM use nonmagnetic materials (e.g., the screws and anchor). Figure 1 shows a block diagram of the OBEM, whereas the specifications of the OBEM comparing with the Japanese system (Kasaya and Goto, 2009) shows in table 1. We designed the data logger, release mechanism, and the OBEM platform to integrate all the sensors or units purchased from related manufactories and focused on the issues of saving power and reducing costs. The detailed requirements of the OBEM are listed below.

1. A magnetic sensor with three axes for measuring magnetic fields
2. A tiltmeter with two axes for measuring leveling changes to correct the tilt error of the magnetic sensor
3. Two pairs of non-polarized electrodes with 2-m bendable arms with a total distance between the electrodes of approximately 4.5 m
4. A highly accurate data logger with at least seven channels and a sampling rate of greater than or equal to 10 samples per second (SPS)
5. Operation time of more than 180 days
6. An internal timing error of less than  $3 \text{ s y}^{-1}$  synchronized with GPS
7. Acoustic relocation and recovery control systems
8. Power consumption of less than 1.5 W
9. A radio beacon, flush beacon, reflect label, and orange flag for identification on the sea surface during instrument recovery
10. A  $0.75 \text{ m s}^{-1}$  subside rate for deployment and float up rate for recovery
11. A maximum deployment depth of more than 6,000 m appropriate for most seawater depths offshore Taiwan

The solutions found for the OBEMs are listed below.

1. A fluxgate with three axes with a sensitivity of  $\pm 70,000 \text{ nT}$ , noise level  $< 6 \text{ pTrms}/\sqrt{\text{Hz}}$  at 1 Hz adding a buffer amplifier with gain=0.2 and passive low pass filter at 50 Hz; the scaling temperature coefficient is  $\pm 15 \text{ ppm}/^\circ\text{C}$ , whereas the offset temperature coefficient is  $\pm 0.1 \text{ nT}/^\circ\text{C}$
2. Four non-polarized electrodes (Ag/AgCl), self-noise level  $< 625 \text{ }\mu\text{V}$  adding a buffer amplifier with gain=20 and two active low pass filter at 50 Hz
3. A tiltmeter with two axes with inclinations of  $\pm 30^\circ$  adding a buffer amplifier gain=0.2 and passive low pass filter at 50 Hz
4. Two pairs of silver chloride electrodes with a 2-m arm-folding mechanism
5. A low noise and low-power consumption eight differential channel 24-bit A/D data logger with an accurate internal timing clock
6. Acoustic transponder and controller units
7. Radio beacon and flash beacon units
8. An OBEM platform modified from that of OBS
9. High-efficiency lithium battery packs for the sensors and data logger

### 3. Units of the OBEM and their specifications

The OBEM is recovered by releasing its anchor from the seafloor via an on-board acoustic command. The OBEM is returned to the sea surface via buoyancy when the anchor is released. There are two typical release mechanisms available for OBEMs to unlock their anchors: spin motor and burn-wire systems (Kasaya and Goto, 2009). The OBEM uses the burn-wire system because it weighs less than the spin motor system. The acoustic controller and transducer use ORE #B980175 ASSY PCB and #D980709, respectively, manufactured by EdgeTech, USA, for the corresponding functions of OBEM recovery and underwater ranging. The ASSY PCB acoustic controller uses a binary FSK encoder, including the commands “RELEASE1,” “RELEASE2,” “DISABLE,” “ENABLE,” and “OPTIONAL1.” The frequency of the acoustic range ranges from 7.5 kHz to 15 kHz in increments of 0.5 kHz with a sensitivity of 80 dB re 1μPa. The #D980709 transducer can work at a depth of 6,000 m and in environments from -10°C to +40°C.

The EdgeTech 8011M model acoustic commander (8011M) is used on board to send the “ENABLE” command to open the ranging function, the “RANGE” command to measure the distance between the OBEM and the research vessel, the “DISABLE” command to close the ranging function, and the “RELEASE1” command to activate the burn-wire system to release the anchor. The “RELEASE1” command persists for 15 min unless terminated by the “OPTIONAL1” command.

We selected the RF-700A and ST-400A NOVATECH models for the radio and flash beacons, respectively, for use in the OBEM. The maximum deployment depth for these models is 7,300 m. The radio beacon is turned ON by sending a VHF signal, and the flush beacon is turned ON at atmospheric pressure of less than 1 atm (equal to a depth of 10 m below the sea surface) in a dark environment. The beacons are also turned OFF at a depth of 10 m or at atmospheric pressure of less than 1 atm, respectively. These two beacons have four independently installed C-type alkaline batteries that allow for six days of continuous operation at maximum; this power supply differs from that of the data logger. The two independent power supply layouts allow the beacons to properly operate even if the power supply for the data logger fails. An on-board radio scanner

detects the signal transmitted from the radio beacon at a distance of 6.4–12.9 km when the OBEM is floating on the surface. These two beacons can assist in locating the OBEM on the sea surface in both daytime and nighttime.

TL-5930 model lithium batteries manufactured by TADIRAN are used for the OBEM, with specifications of 3.6 V, 19 Ah, and D-type with characteristics of high energy density and a low self-discharge rate suitable for long periods of operation. Figure 2 shows a block diagram of the OBEM data logger. The ADC1278EVM model is a 24-bit A/D converter used for the inputs of the three fluxgate axes, the two tiltmeter axes, and two pairs of non-polarized electrodes with a sampling rate of 10 SPS. An amplifier and a low-pass filter (Amp & LPF) were designed for the magnetic sensor, leveling sensor, and electric receiver inputs. The two MPS430F5436A microcontrollers (MCU) process the timing synchronization of the time base manufactured by SeaSCAN, USA, and the GPS modules; the digital data is stored to a Secure Digital (SD) memory card with a standard Secure Digital High Capacity (SDHC), and the user interface communicates with a PC. The time base module supplies a precise time base signal to the data logger, whereas the SISMTB Ver 4.1 time base module generates a precise 125-Hz clock that supports a timing error smaller than  $3 \text{ s y}^{-1}$ . Even though the time base module supports a very small timing error of  $3 \text{ s y}^{-1}$ , the data logger clock is still synchronized with the GPS on deck for timing corrections after recovering the OBEM. The maximal capacity of the SD card is 64 GB and can support data storage for more than one year with a sampling rate of 10 SPS.

Two 17-in glass VITROVEX spheres manufactured by Nautilus Marine Service GmbH, Germany, are used for the OBEM. These glass spheres contain the fluxgate and tiltmeter (sensor ball) and the seven channels of the Amp & LPF, data logger, #B980175 ASSY PCB acoustic controller, and batteries (instrument ball) and can be deployed at a depth of 6,000 m and support a total buoyancy of 52 kg. The instrument and sensor balls, the silver chloride electrodes, and the burn-wire system are connected via waterproof cables. There is a pressure-vacuum valve outside the glass spheres that allows a pumped vacuum to be preserved at 0.7 atm; self-fusing butyl rubber tape is used to fill the suture zone between the half glass spheres. In addition, two crossed stainless-steel bands are used to improve the waterproofing of the glass spheres and cover the orange PE cases.

Four PVC pipes with lengths of 2 m are combined to form the OBEM platform for the electric receivers, and the silver chloride electrodes are installed at the ends of the pipes. A 60-kg nonmagnetic anchor is attached to the bottom of the OBEM platform and catches via a releasing mechanism. The anchor can be released using the burning-wire system to recover the OBEM. Figure 3 shows a photograph of the OBEM platform.

## 4. Calibrations of the OBEM

It is necessary to calibrate each unit of the OBEM, including the data logger with the Amp & LPF, fluxgate, tiltmeter, electrodes, ASSY PCB acoustic controller, transducer, and wiring, before and after assembling the OBEM to improve its performance. We describe the series of calibration methods used for the OBEM units in the following section.

### 4.1 Calibrations of the background noise of the data logger and the Amp & LPF

The background noise of the data logger is defined as

$$N_{rms} = \sqrt{\frac{1}{n}(A_1^2 + A_2^2 + \dots + A_n^2)}, \quad (1)$$

where  $n$  is a data point and  $A_1$  to  $A_n$  indicate the amplitudes of the data points, 1 to  $n$ , individually at the short circuit or 0 V. The background noise of the data logger (in “BIT”) is calculated as

$$dB_{rms} = 20 \log_2(N_{rms}), \quad (2)$$

The data logger contains seven input channels called MX, MY, MZ, TX, TY, EX, and EY. MX, MY, and MZ are used for the magnetic sensor of the fluxgate, TX and TY are used for the tiltmeter, and EX and EY are used for the electric receivers. The calibration procedure is described below.

1. Connect MX, MY, MZ, TX, and TY to GND, EX+ with EX-, and EY+ with EY-.
2. Start the record mode of the data logger, wait for 60 s to acquire data, and then stop recording data.
3. Download the data from the data logger and convert it to ASCII format. Then, calculate the background noise using Eq. (1) and the background noise in dB using Eq. (2).

## 4.2 Calibrations of the sensitivity, linearity error, and dynamic range for the data logger and the Amp & LPF

The input ranges of the voltages for MX, MY, and MZ are  $\pm 10$  V, for TX and TY are  $\pm 5$  V, and for EX and EY are  $\pm 0.00625$  V. The sensitivities are calculated from the average count of the input voltages, that is, subtract the average count at zero voltage and then divide by the input voltages:

$$S = \text{Average} \left( \frac{\text{Average}(C_i) - \text{Average}(C_0)}{V_i} \right), \quad (3)$$

where  $V_i$  is the input voltage,  $C_i$  is the output count saved on the SD card for an input voltage of  $V_i$ , and  $C_0$  is the output count saved on the SD card for an input voltage of 0 V.

The linearity errors are calculated such that

$$\text{Error} = \text{Abs} \left[ \frac{S_i - S_T}{S_T} \right] \times 100, \quad (4)$$

where  $S_i$  is the sensitivity of the input voltage and  $S_T$  is the total sensitivity.

The dynamic range is the ratio of the maximum count to the background noise. It is defined as

$$D = 20 \log \left( \frac{S_T \times V_{\max}}{N_{\text{RMS}}} \right), \quad (5)$$

where  $S_T$  is the total sensitivity and  $V_{\max}$  is 10 V for MX, MY, and MZ, 5 V for TX and TY, and 0.00625 V for EX and EY. Its calibration procedure is described below.

1. Connect the MX, MY, and MZ channels of the data logger to the source voltages generated by the calibrator (FLUKE726) and connect the GND channel of the data logger to the source common point (COM) of FLUKE726.
2. Set the data logger to the recording mode.
3. Set the FLUKE726 output voltages from 0 V to  $\pm 10$  V. Increase and decrease the voltages step by step in 1 V intervals until  $\pm 10$  V. The measurement time length for each output voltage is 20 s.
4. Connect the TX and TY channels of the data logger to the source voltages generated by FLUKE726 and connect the GND channel of the data logger to COM of FLUKE726.



5. Set the FLUKE726 output voltages from 0 V to  $\pm 5$  V. Increase and decrease the voltages step by step in 1 V intervals until  $\pm 5$  V. The measurement time length for each output voltage is 20 s.
6. Connect the EX+ and EY+ channels of the data logger to the source voltages generated by FLUKE726, and connect the EX- and EY- channels of the data logger to COM of FLUKE726.
7. Set the FLUKE726 output voltages from 0 V to  $\pm 6$  mV. Increase and decrease the voltages step by step in 1-mV intervals until  $\pm 6$  mV. The measurement time length for each output voltage is 20 s.
8. Finally, switch off the recording mode of the data logger, download the data, and convert it to ASCII format for analysis. Calculate the sensitivity, linearity error, and dynamic range using Eqs. (3), (4), and (5), respectively.

Figure 4 shows a calibration of the magnetic channels (MX, MY, and MZ) checking the sensitivity, linearity, and error. The average sensitivity is 655,968.5 counts/V with a maximum error smaller than 1.35%. Figure 5 shows a calibration of the electric channels (EX and EY) checking the sensitivity, linearity, and error. The average sensitivity is 135,856,047.8 counts/V with a maximum error smaller than 0.8%. Figure 6 shows a calibration of the tiltmeter channels (TX and TY) checking the sensitivity, linearity, and error. The average sensitivity is 1,677,710.6 counts/V with a maximum error smaller than 0.25%. The noise level of the data logger is 57.8 dB, whereas its dynamic range is 80.2 dB at 10 Hz.

### 4.3 Evaluation of the current consumption

The power supplies of the OBEM consist of two 7.2-V battery packs in a series connection with two 3.6-V lithium batteries. One battery pack is for the data logger and converts to  $\pm 5$  VDC and +3.3 VDC. The other pack is for the sensors and converts to  $\pm 5$  VDC and +12.0 VDC. Two +7.4-VDC output current batteries were measured for their current consumption measurement using two ammeters connecting the two +7.4-V battery packs. Table 2 shows the current consumption of the OBEM system. The maximum current consumptions of the data logger and sensors are 32 mA and 105 mA, respectively. The total power consumption is less than 1 W, which corresponds to expectations.

#### 4.4 Evaluation of the electrodes

Two pairs of silver chloride electrodes are used for the OBEM. We first put a pair of electrodes separated by a fixed distance within a tank filled with seawater to check the status of the electrodes. Second, we measured the electrical potential and impedance of the electrodes using a digital volt-ohm-milliammeter (VOM) (Fig. 7). Third, we sent a swept sine signal to check the frequency responses of the electrodes, as shown in Fig. 8. Fourth, we input a DC voltage to check the electrode-induced voltages, as shown in Fig. 9. Table 3 shows the self-potential, impedance, and induced voltages for each pair of electrodes. The ranges of the self-potential and impedance are 0.26–3.63 mV and 243–370  $\Omega$ , respectively. The electrical potential shows that 81–167 mV was transmitted from the 5 VDC of the two copper electrodes.

#### 4.5 Evaluation of the fluxgate

The fluxgate is mounted in the sensor ball of the OBEM. Therefore, we could only calculate the total magnetic field (TMF) (Eq. (6)) measured from the three components of the fluxgate. We then compared the difference between the TMF of the OBEM and geomagnetic data of the geophysical database management system from the Central Weather Bureau. The TMF is calculated by

$$M_T = \sqrt{(M_X^2 + M_Y^2 + M_Z^2)}, \quad (6)$$

where  $M_X$ ,  $M_Y$ , and  $M_Z$  are the components of the north-south, east-west, and vertical magnetic fields, respectively.

#### 4.6 Evaluation of the acoustic transceiver and its transducer

We selected the large-scale Breeze Canal in New Taipei City for testing because it has few obstacles and is suitable for evaluating the functions of the 8011M. The Breeze Canal has a length of approximately 800 m and is located in a straight river with a depth of 2–5 m. The distance between the transducer and the acoustic transceiver was approximately 630 m, and the layout for the field test is shown in Fig. 10. The testing procedure for the transducers is described below. The results are listed in Table 4.

1. Connect the tested transducer and acoustic transceiver via an underwater cable, and place the tested transducer and transceiver at an underwater depth of 1 m.

- 293 2. Record the serial numbers of the transducers in a notebook.
- 294 3. Send the "ENABLE" command via the 8011M, and then count the response
- 295 beeps.
- 296 4. Send the "RANGE" command via the 8011M five times, and record the distance
- 297 of each ranging.
- 298 5. Send the "DISABLE" command via the 8011M, and then count the response
- 299 beeps.
- 300 6. Replace the transducer, and return to step 2 to repeat the evaluation.

301

302 We then checked the acoustic transceivers after all of the transducers were successfully  
303 checked; the testing procedure for the acoustic controller is described below. The results  
304 are listed in Table 5.

- 305 1. Change the acoustic controller, and record its serial number in a notebook.
- 306 2. Send the "ENABLE" command via the 8011M, and then count the response
- 307 beeps.
- 308 3. Send the "RANGE" command via the 8011M five times, and record the distance
- 309 of each ranging.
- 310 4. Send the "RELEASE1" command via the 8011M, and then count the response
- 311 beeps. Check the voltage between Pin1 and Pin2 of JP2 using a VOM. It should
- 312 be greater than 12.0 VDC.
- 313 5. Send the "OPTION1" command via the 8011M, and then count the response
- 314 beeps. Check the voltage between Pin1 and Pin2 of JP2 using a VOM. It should
- 315 be 0 VDC.
- 316 6. Send the "RELEASE2" command via the 8011M, and then count the response
- 317 beeps. Check the voltage between Pin3 and Pin4 of JP2 using a VOM. It should
- 318 be greater than 12.0 VDC.
- 319 7. Send the "OPTION1" command via the 8011M, and then count the response
- 320 beeps. Check the voltage between Pin3 and Pin4 of JP2 using a VOM. It should
- 321 be 0 VDC.
- 322 8. Send the "DISABLE" command via the 8011M, and then count the response
- 323 beeps.
- 324 9. Send the "RANGE" command via the 8011M; there should be no response from
- 325 the transceiver.

10. Return to step 1 to repeat the evaluation.

A mercury switch is mounted on the transceiver which when turned off responds with 15 beeps and when turned on responds with seven beeps.

## **5. The preliminary result of the OBEM offshore Taiwan**

We deployed six broadband BBYBs and one OBEM near a small submarine volcano area in the OT offshore NE Taiwan (Fig. 11) on 03/26/2018 for a submarine observation to evaluate all the OBEM units. All the equipment was successfully recovered after one month of deployment. Figure 12 shows the time series of data of OBEM01. The TMF calculated from the three components of the magnetic field varied in the range of 44,100–4,4150 nT, which corresponded to the geomagnetic field measured by proton magnetometers in Taiwan. The two horizontal magnetic fields contained significant daily variations. Furthermore, the vibrations of the inclinations were significantly affected by two earthquakes on 04/27/2018 (at 12:41 UTC and 12:47 UTC) consistent with seismic signals of the BBYBs (Fig. 13). The average magnetic fields of HX, HY, HZ, and TMF 2 s prior to the earthquakes (12:41 UTC) were 12,900 nT, 34,300 nT, 24,600 nT, and 44137 nT, respectively, the average potential fields of EX and EY were  $-0.79$  mV and  $-0.149$  mV, respectively, and the inclinations of TX and TY were  $-2.65^\circ$  and  $1.21^\circ$ , respectively. These were the averages of the background without earthquakes.

We subtracted the background averages of the magnetic fields and the inclinations to compare the differential during the 12:41 UTC event as shown in Fig. 14. The peak ground motion velocity (PGV) was  $2.63 \text{ cm s}^{-1}$  on the SH1 corresponding to inclinations of  $0.4^\circ$  and  $0.6^\circ$  for TX and TY with a 100 nT disturbance of HY. There was an insignificant amount of variation in the electric fields. The result shows that the earthquake significantly affected the HY component, whereas Hx and Hz components also slightly affected by the earthquake. It could be related to the orientations of the magnetic sensor and the earthquake.

## **6. Conclusions**

A long-period OBEM acquisition platform to measure magnetic and electrical fields on the seafloor was successfully constructed and evaluated by the OBS R&D team for

deployment offshore Taiwan. The power consumption of the OBEM is less than 1 W, which means that the lifetime could be extended up to 300 days with the installation of 108 lithium batteries. We deployed and recovered the OBEM at an underwater depth of 1,400 m to acquire the first marine magnetotelluric data offshore NE Taiwan.

Six broadband BBYBs and one OBEM were deployed near a small submarine volcano area offshore NE Taiwan. The TMF calculated from the three magnetic field components varied in the range of 44,100–4,4150 nT, which corresponded to the proton magnetometer measurements of the geomagnetic field in Taiwan. The two horizontal magnetic fields displayed significant daily variations, and the vibrations of the inclinations were significantly affected by the two earthquakes that occurred during the observations. There was an insignificant amount of variation in the electric fields.

Localized micro-earthquakes affected the disturbances of the magnetic field and inclinations in this study. Therefore, to improve the efficacy of marine geophysical explorations, a platform for multiple underwater measurements is required including an ocean bottom flow meter, thermometer, and absolute pressure gage. We will focus on such developments, in which the evaluated results show that the data logger, flush and radio beacons, EMI filter, and an integrated junction board must be improved relating noise levels, cost, and convenient maintenance issues in the future.

## **Acknowledgments**

We greatly appreciate the crews of R/V OR2 for the field experiments. The authors acknowledge the financial support from the Ministry of Science and Technology of Taiwan under grant numbers of 105-2116-M-019-001, 106-2116-M-001-008, 106-2116-M-019-003, 107-2116-M-019-006, 108-2116-M-001-012, and 108-2116-M-019-006. We also thank four years of the Taiwan-German cooperative projects on gas hydrate of NEPII for supporting the funds of the instrument deployment of the OBEMs. We would like to thank the TEC Data Center for providing graphical services.

## **References**

Bertrand, E., Unsworth, M., Chiang, C. W., Chen, C. S., Chen, C. C., Wu, F., Turkoglu, E., Hsu, H. L., and Hill, G.: Magnetotelluric evidence for thick-skinned tectonics

391 in central Taiwan, *Geology*, 37, 711-714, 2009.

392 Bertrand, E. A., Unsworth, M. J., Chiang, C. W., Chen, C. S., Chen, C. C., Wu, F. T.,  
393 Turkoglu, E., Hsu, H. L., and Hill, G. J.: Magnetotelluric imaging beneath the  
394 Taiwan orogen: An arc-continent collision, *J Geophys Res-Sol Ea*, 117, 2012.

395 Chiang, C. W., Chen, C. C., Unsworth, M., Bertrand, E., Chen, C. S., Kieu, T. D., and  
396 Hsu, H. L.: Corrigendum to “The deep electrical structure of southern Taiwan and  
397 its tectonic implications”, *Terr. Atmos. Ocean Sci.*, 22, 371-371, 2011.

398 Chiang, C. W., Chen, C. C., Unsworth, M., Bertrand, E., Chen, C. S., Thong, D. K., and  
399 Hsu, H. L.: The deep electrical structure of southern Taiwan and its Tectonic  
400 Implications, *Terr. Atmos. Ocean Sci.*, 21, 879-895, 2010.

401 Chiang, C. W., Hsu, H. L., and Chen, C. C.: An investigation of the 3D electrical  
402 resistivity structure in the Chingshui geothermal area, NE Taiwan, *Terr. Atmos.*  
403 *Ocean Sci.*, 26, 269-281, 2015.

404 Chiang, C. W., Unsworth, M. J., Chen, C. S., Chen, C. C., Lin, A. T. S., and Hsu, H. L.:  
405 Fault zone resistivity structure and monitoring at the Taiwan Chelungpu Drilling  
406 Project (TCDP), *Terr. Atmos. Ocean Sci.*, 19, 473-479, 2008.

407 Ellis, M., Evans, R. L., Hutchinson, D., Hart, P., Gardner, J., and Hagen, R.:  
408 Electromagnetic surveying of seafloor mounds in the northern Gulf of Mexico,  
409 *Mar. Pet. Geol.*, 25, 960-968, 2008.

410 Evans, R. L., Hirth, G., Baba, K., Forsyth, D., Chave, A., and Mackie, R.: Geophysical  
411 evidence from the MELT area for compositional controls on oceanic plates, *Nature*,  
412 437, 249-252, 2005.

413 Google Maps: Retrieved from  
414 [https://www.google.com.tw/maps/@25.0902745,121.4516598,1296m/data=!3m](https://www.google.com.tw/maps/@25.0902745,121.4516598,1296m/data=!3m1!1e3?hl=zh-TW)  
415 [1!1e3?hl=zh-TW](https://www.google.com.tw/maps/@25.0902745,121.4516598,1296m/data=!3m1!1e3?hl=zh-TW), 2019.

416 Kasaya, T. and Goto, T.: A small ocean bottom electromagnetometer and ocean bottom  
417 electrometer system with an arm-folding mechanism, *Explor. Geophys.*, 40, 41-  
418 48, 2009.

419 Key, K.: Marine Electromagnetic Studies of Seafloor Resources and Tectonics, *Surv.*  
420 *Geophys.*, 33, 135-167, 2012.

421 Kuo, B. Y., Crawford, W. C., Webb, S. C., Lin, C. R., Yu, T. C., and Chen, L. W.:  
422 Faulting and hydration of the upper crust of the SW Okinawa Trough during  
423 continental rifting: Evidence from seafloor compliance inversion, *Geophys. Res.*

424 Lett., 42, 4809-4815, 2015.  
 425 Kuo, B. Y., Wang, C. C., Lin, S. C., Lin, C. R., Chen, P. C., Jang, J. P., and Chang, H.  
 426 K.: Shear-wave splitting at the edge of the Ryukyu subduction zone, Earth Planet.  
 427 Sci. Lett., 355, 262-270, 2012.  
 428 Kuo, B. Y., Webb, S. C., Lin, C. R., Liang, W. T., and Hsiao, N. C.: Removing  
 429 infragravity-wave-induced noise from Ocean-Bottom Seismographs (OBS) data  
 430 deployed offshore of Taiwan, Bull. Seismol. Soc. Am., 104, 1674-1684, 2014.  
 431 Utada, H.: Electromagnetic exploration of the oceanic mantle, P Jpn Acad B-Phys, 91,  
 432 203-222, 2015.

## TABLE AND FIGURE CAPTIONS

Table 1. Specifications of the OBEM comparing with the Japanese OBEM and OBE (Kasaya and Goto, 2009)

Table 2. The total current consumption of the OBEMs.

Table 3. The self-potential, impedance, and induced voltage results for each pair of silver chloride electrodes.

Table 4. Example results for the functional test of the acoustic transducer.

Table 5. Example results for the functional test of the acoustic controller.

Figure 1. A block diagram of the OBEM. The inputs of the two electric fields, two inclinations, and three magnetic fields pass through the Amp & LPF in the data logger, which contains a 64-GB SD card. The SeaSCAN time base module is integrated into the data logger and has a timing error smaller than  $3 \text{ s y}^{-1}$ . The EdgeTech acoustic transceiver and transducer are used for the positioning and releasing of the anchor. The radio and flash beacons are used to locate the OBEM at the sea surface during recovery operations.

Figure 2. A block diagram of the OBEM data logger. The ADS1278EVM is a 24-bit A/D with eight inputs used for converting analog signals via the amplifier and low-pass filter (Amp & LPF) to digital data. The Amp & LPF adjusts the output voltages of the sensors of the fluxgate, tiltmeter, and electric receivers to suitable A/D input levels. The two MCUs of the MPS430F5436A process the timing synchronization by the SeaSCAN of time base and GPS modules, the digital data storage to the SD card with a standard SDHC, and the user interface communication with a PC.

Figure 3. A photograph of the OBEM01 and its specific modules.



Figure 4. Calibration results for the magnetic channels of the OBEM01. (a) Linearity, (b) sensitivity, and (c) error. The average sensitivity is 655,968.5 counts/V, and the maximum error is <1.35%.

Figure 5. Calibration results for the electric channels of the OBEM01. (a) Linearity, (b) sensitivity, and (c) error. The average sensitivity is 1,358,568,047.8 counts/V, and the maximum error is <0.8%.

Figure 6. Calibration results for the inclination channels of the OBEM01. (a) Linearity, (b) sensitivity, and (c) error. The average sensitivity is 1,677,710.6 counts/V, and the maximum error is <0.25%.

Figure 7. The layout for the evaluation of the electric receivers. Two copper electrodes are used to vary the input signals. A pair of silver chloride electrodes are placed at the corner of a tank with an area of 68 cm × 49 cm filled with 15 cm of seawater. A VOM is used to measure the self-potential and impedance of the electrodes.

Figure 8. The responses of the electrodes with varying frequencies. The response curves of  $V_o/V_i$  are proportional to the frequency on a log scale.

Figure 9. The responses of the electrodes with varying voltages. The input was ranged from 500 mVDC to 2,500 mVDC to check the induced voltage; the induced voltages are proportional to the input voltages.

Figure 10. A map of the field test to evaluate the acoustic transducer, acoustic controller, and 8011M (modified from Google map, 2019).

Figure 11. A location map showing the BBYBs and OBEM with triangle and diamond symbols, respectively.

Figure 12. The OBEM01 time series data. The panels from top to bottom in the figure show the four magnetic fields: TMF, HX, HY, and HZ, the two electric fields: EX and EY, and the two inclinations: TX and TY.

498

499 Figure 13. Comparison of the OBEM01 and 1802OBS time series data during the two  
500 earthquakes. The two earthquakes affected the inclinations. The first and secondary  
501 earthquakes occurred at 12:41 UTC and 12:47 UTC, respectively, on 04/27/2018. SH1  
502 and SH2: two horizontal components of the seismic signal; SZ: vertical component of  
503 the seismic signal.

504

505 Figure 14. The variations in PGV, TMF, HY, TX, and TY during the first earthquake.  
506 The PGV of 2.63 cm/s affected the inclinations by  $0.601^\circ$  and  $0.404^\circ$  for TX and TY,  
507 respectively, and the HY magnetic field had a peak of 100 nT. SH1 and SH2: two  
508 horizontal components of the seismic signal; SZ: vertical component of the seismic  
509 signal.

## TABLES AND FIGURES

Table 1

|   | Taiwan (OBEM)   | Japan (OBEM)    | Japan (OBE)                 |
|---|-----------------|-----------------|-----------------------------|
| Sampling rate (Hz)                      | 10              | 8               | 1                           |
| AD converter (bits)                     | 24              | 16              | 24                          |
| Resolution ( $\mu\text{V}/\text{LSB}$ ) | 1.5245          | 0.305176        | 0.0019                      |
| Resolution of magnetic field (nT/LSB)   | 0.010671        | 0.01            | none                        |
| Max. battery lifetime                   | About 180 days  | About 40 days   | About 30 days               |
| Power supply                            | Lithium battery | Lithium battery | Li-ion rechargeable battery |
| Max. memory/Media                       | 64 GB/ SD card  | 2GB/ CF card    | 1GB/ CF card                |
| Communication port                      | USB 2.0         | USB1.1/RS-232C  | RS-232C                     |
| Clock drift                             | < 0.95 ppm      | < 2 ppm         | < 2 ppm                     |

Table 2

| Logger S/N | Turn-on Mode (mA)    |                  |                   | Recording Mode (mA)  |                  |                   |
|------------|----------------------|------------------|-------------------|----------------------|------------------|-------------------|
|            | 7.2V for Data logger | 7.2V for Sensors | Power consumption | 7.2V for Data logger | 7.2V for Sensors | Power consumption |
| OBEM01     | 32                   | 104              | 0.98              | 31                   | 105              | 0.98              |
| OBEM02     | 30                   | 94               | 0.89              | 29                   | 97               | 0.91              |
| OBEM03     | 29                   | 103              | 0.95              | 29                   | 104              | 0.96              |

Table 3

|            | Electrical potential | Impedance    | Input DC5V, induce voltage |
|------------|----------------------|--------------|----------------------------|
| OBEM01(EX) | 0.56 mV              | 245 $\Omega$ | 164 mV                     |
| OBEM01(EY) | 0.26 mV              | 272 $\Omega$ | 167 mV                     |
| OBEM02(EX) | 3.63 mV              | 243 $\Omega$ | 81 mV                      |
| OBEM02(EY) | 1.93 mV              | 370 $\Omega$ | 95 mV                      |
| OBEM03(EX) | 2.38 mV              | 267 $\Omega$ | 83 mV                      |
| OBEM03(EY) | 2.1 mV               | 331 $\Omega$ | 83 mV                      |

Table 4

| Transducer S/N | Enable Beep (Times) | Disable Beep (Times) | 1st Ranging Distance show on 8011M (m) | 2nd Ranging Distance show on 8011M (m) | 3rd Ranging Distance show on 8011M (m) | 4th Ranging Distance show on 8011M (m) | 5th Ranging Distance show on 8011M (m) | Judgment |
|----------------|---------------------|----------------------|--|--|--|--|--|----------|
| 35427          | 15                  | 15                   | 629                                    | 628                                    | 630                                    | 627                                    | 628                                    | Good     |
| 35428          | 15                  | 15                   | 629                                    | 627                                    | 629                                    | 630                                    | 629                                    | Good     |
| 35429          | 15                  | 15                   | 630                                    | 630                                    | 630                                    | 629                                    | 629                                    | Good     |

Table 5

| S/N   | Enable Beep (Times) | 1st Ranging Distance show on 8011M (m) | 2nd Ranging Distance show on 8011M (m) | 3rd Ranging Distance show on 8011M (m) | 4th Ranging Distance show on 8011M (m) | 5th Ranging Distance show on 8011M (m) | RELEASE1 Beep Times/Volt | OPTION1 Beep (Times) | RELEASE2 Beep Times/Volt | OPTION1 Beep (Times) | DISABLE Beep (Times) |
|-------|---------------------|--|--|--|--|--|--------------------------|----------------------|--------------------------|----------------------|----------------------|
| 50854 | 15                  | 628                                    | 629                                    | 630                                    | 630                                    | 630                                    | 15/<br>12.77V            | 15                   | 15/<br>12.77V            | 15                   | 15                   |
| 50784 | 7                   | 629                                    | 630                                    | 630                                    | 630                                    | 630                                    | 7/ 12.77V                | 7                    | 7/<br>12.77V             | 7                    | 7                    |
| 50783 | 15                  | 628                                    | 628                                    | 628                                    | 629                                    | 631                                    | 15/<br>12.77V            | 15                   | 15/<br>12.77V            | 15                   | 15                   |

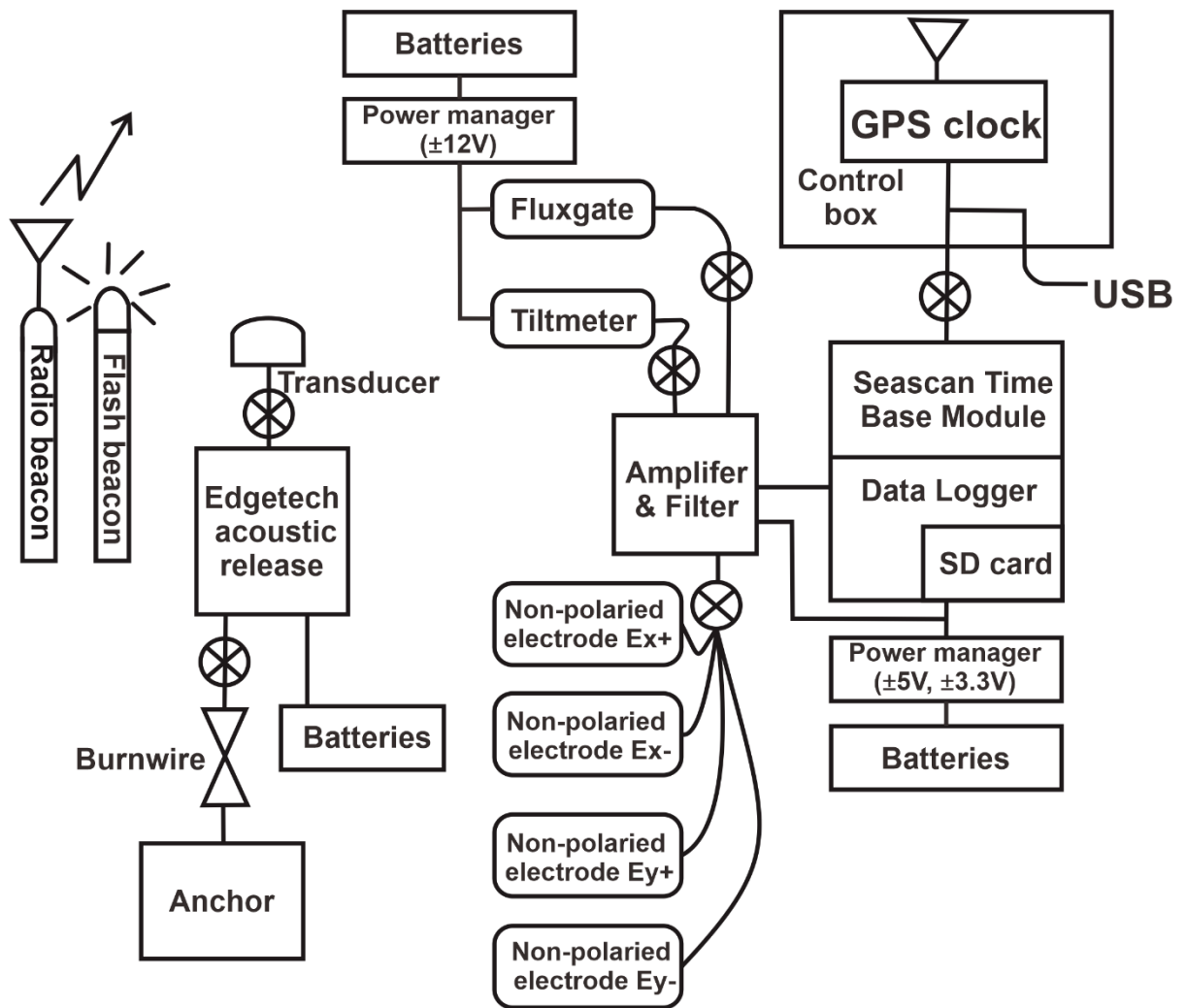


Figure 1

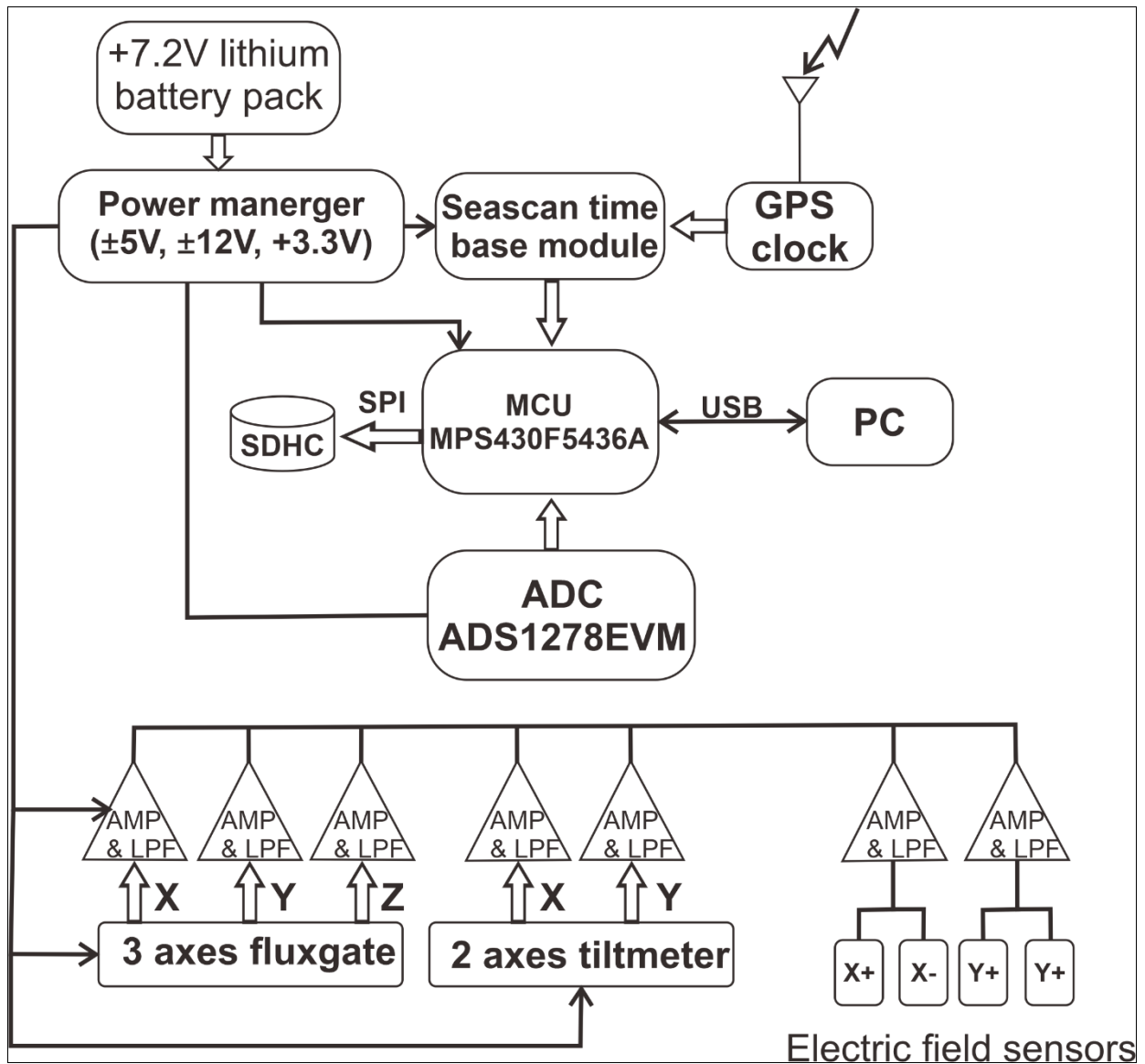


Figure 2

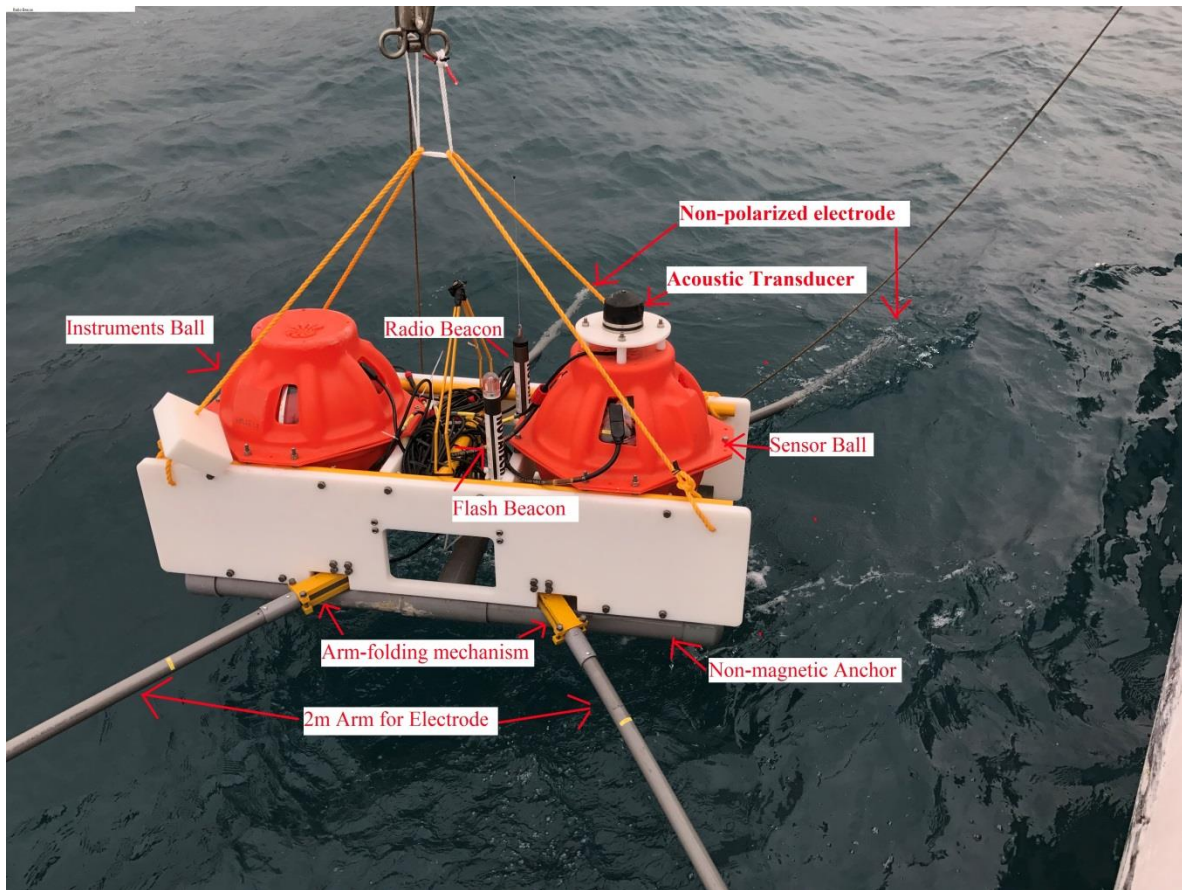
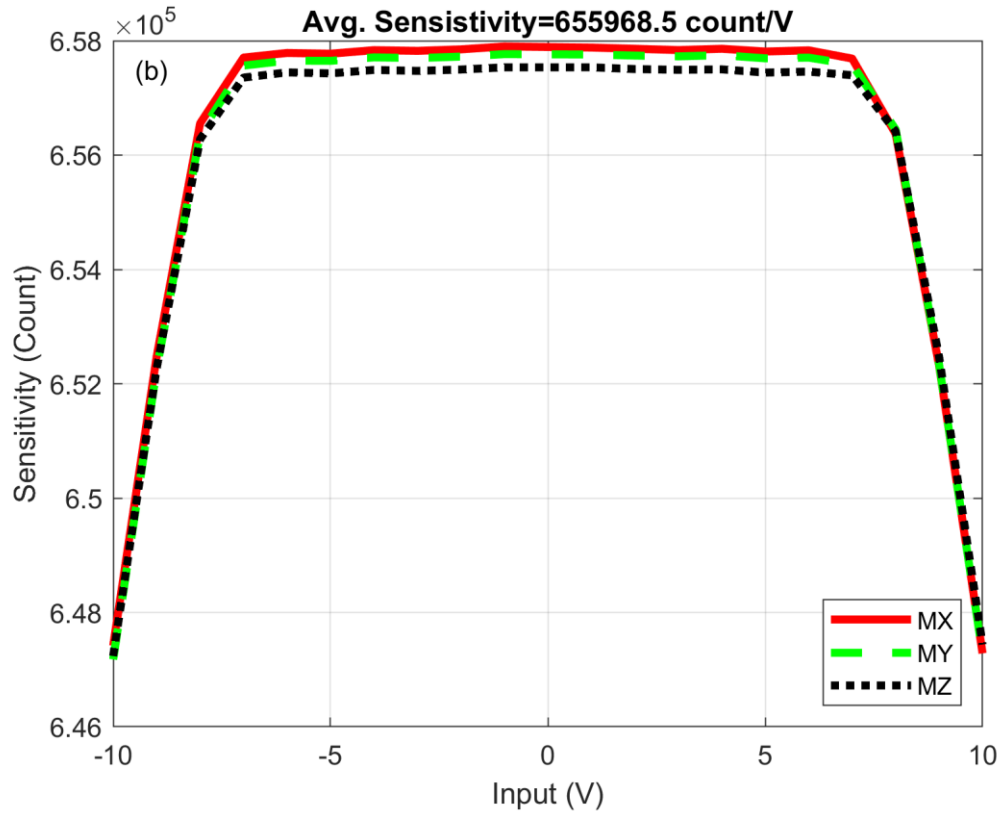
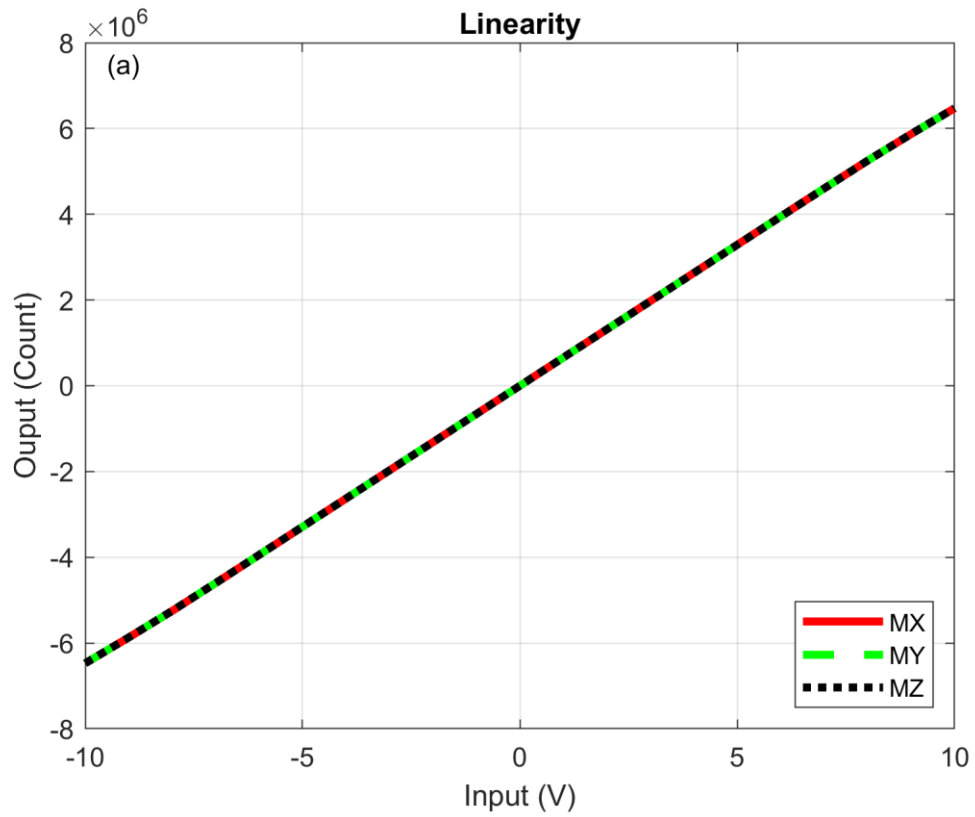


Figure 3





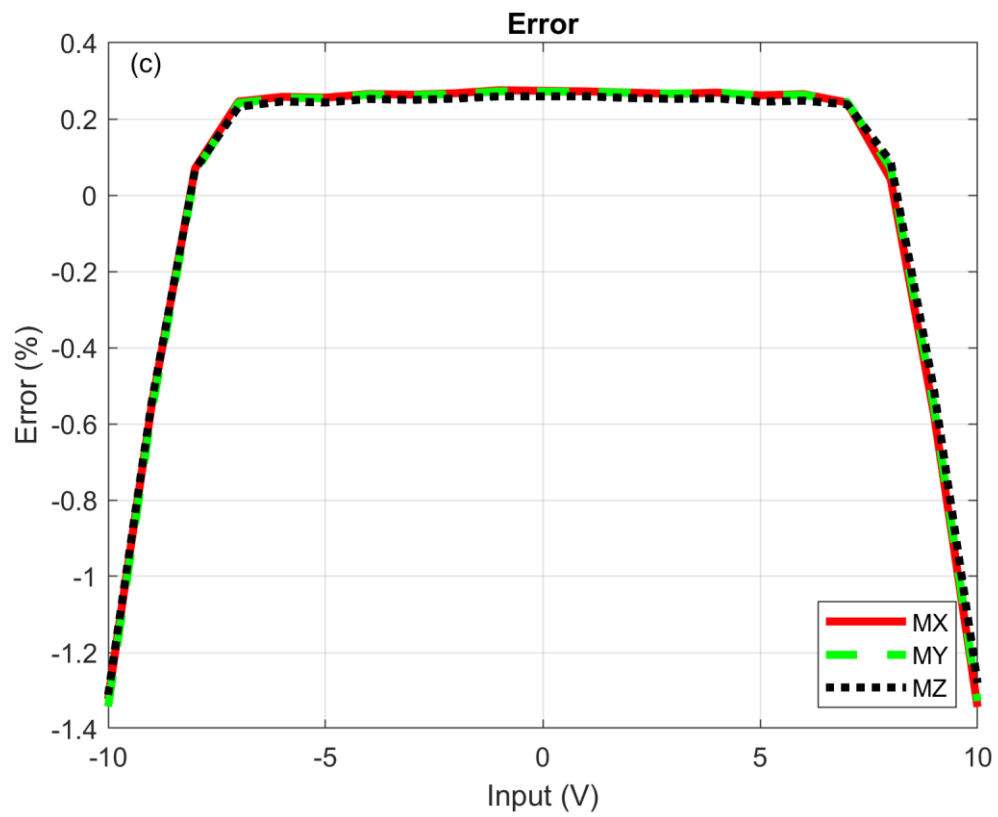
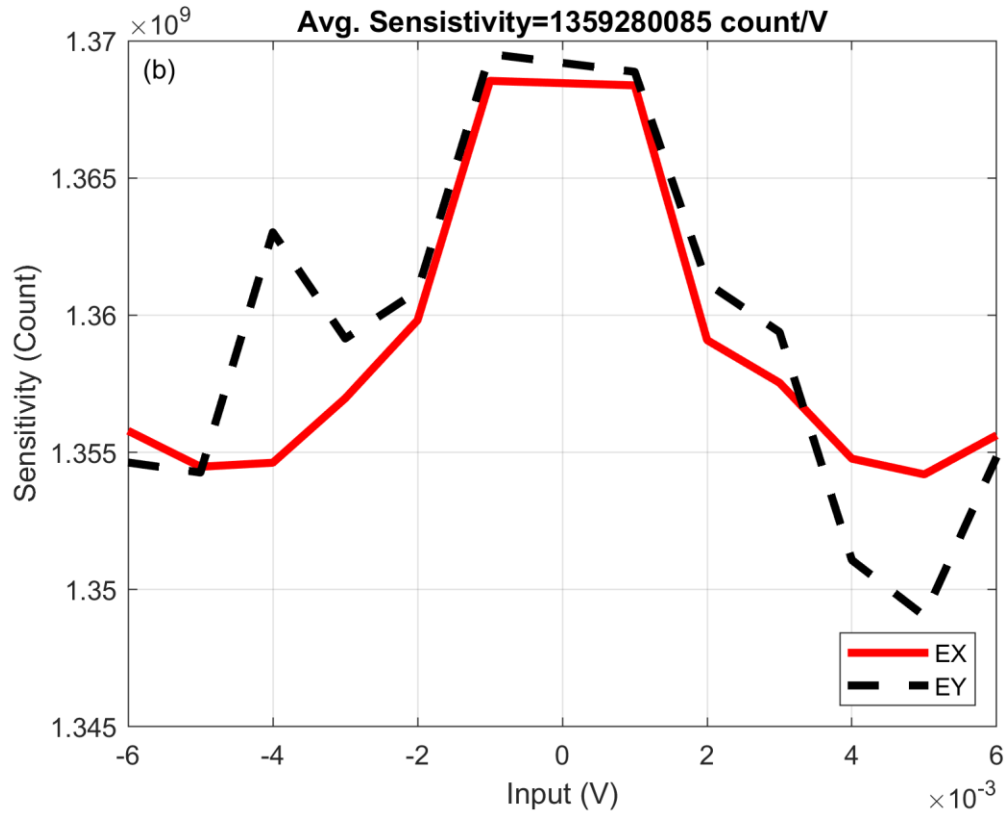
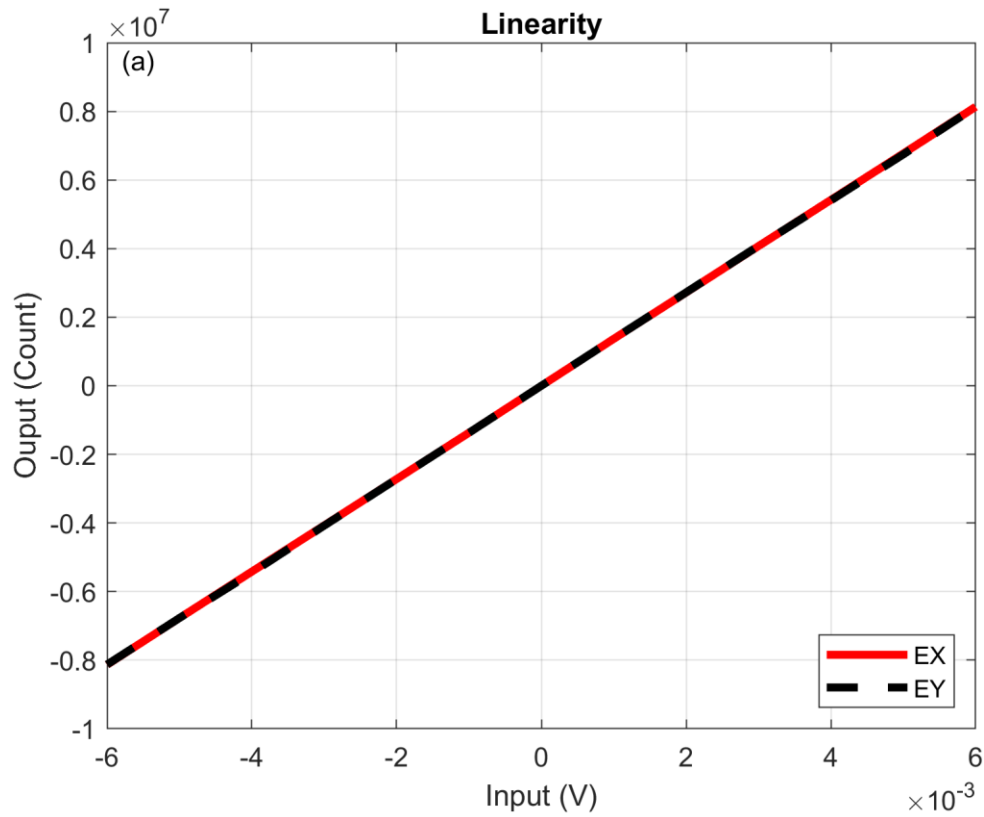


Figure 4



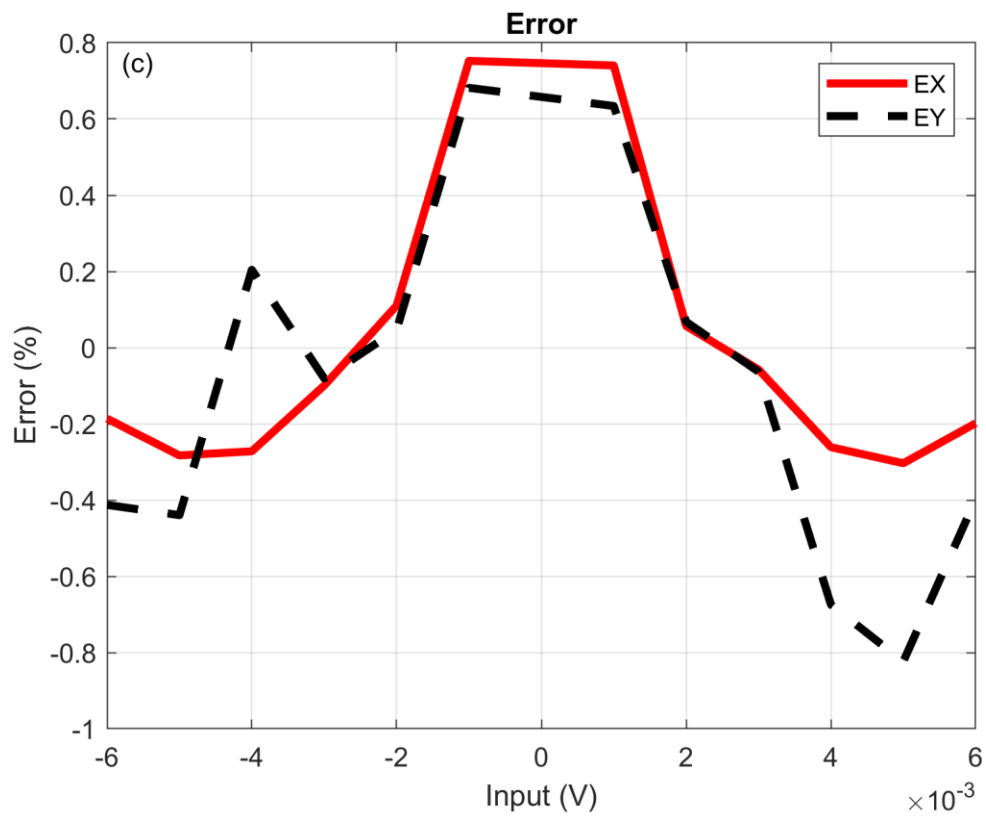
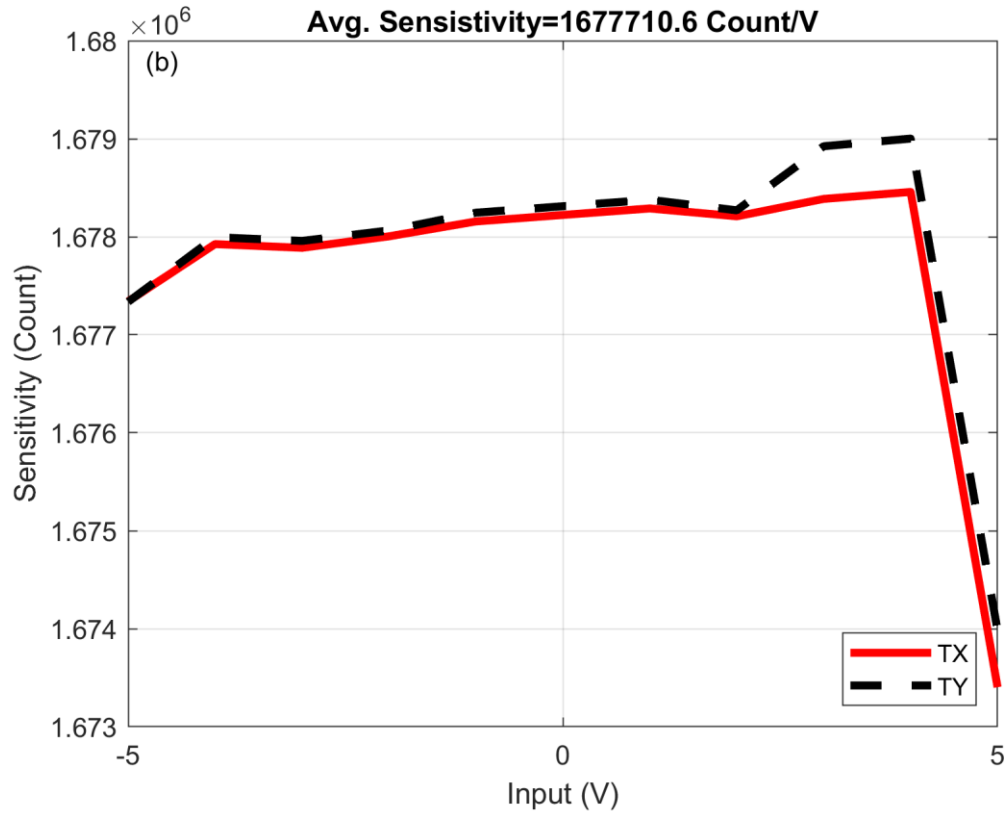
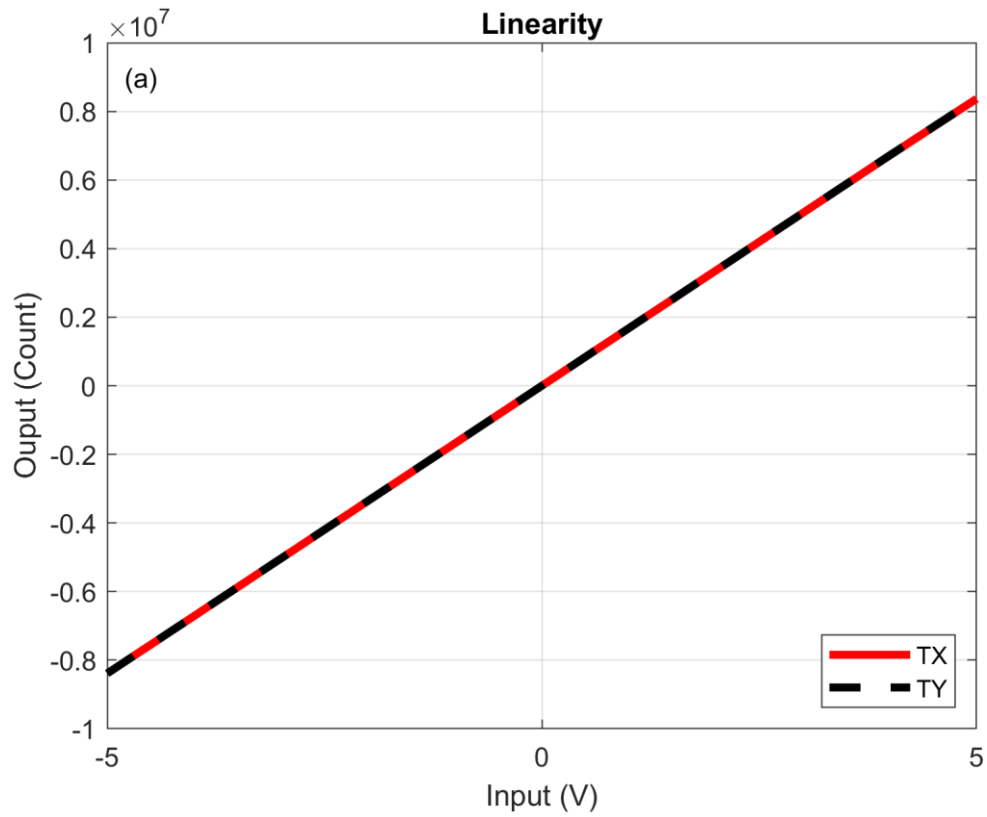


Figure 5



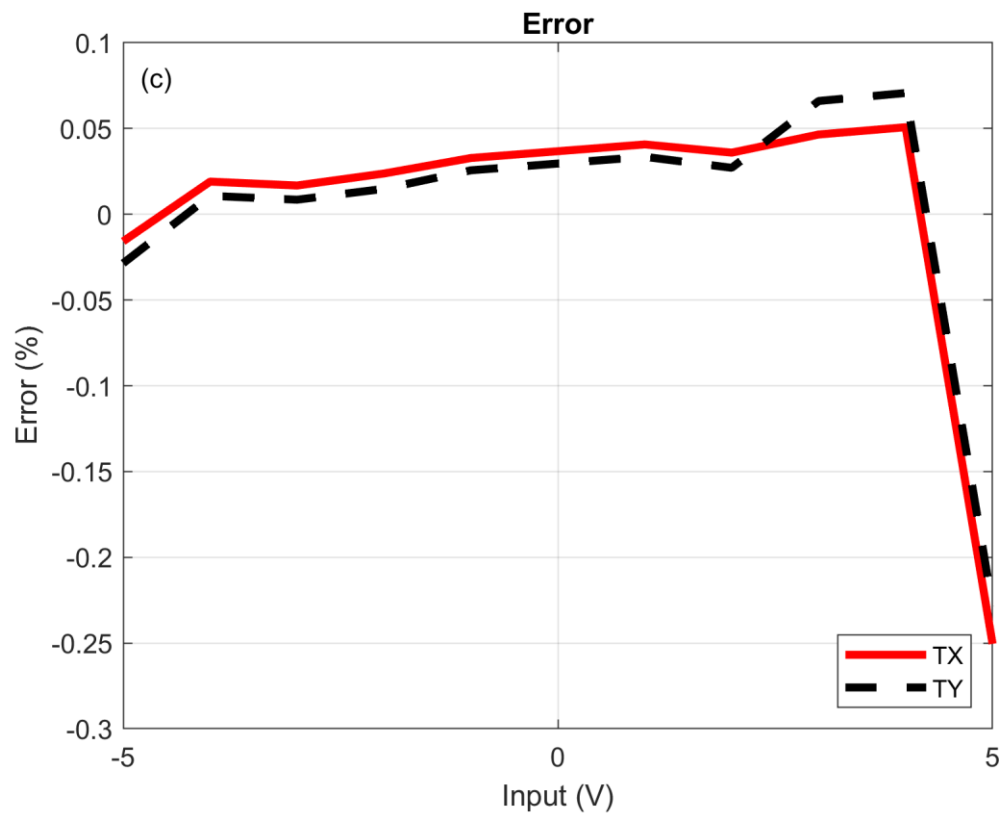


Figure 6

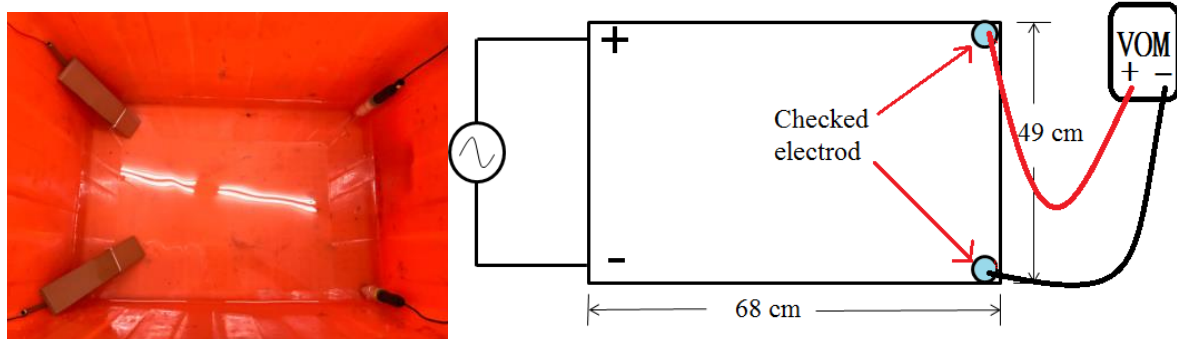


Figure 7

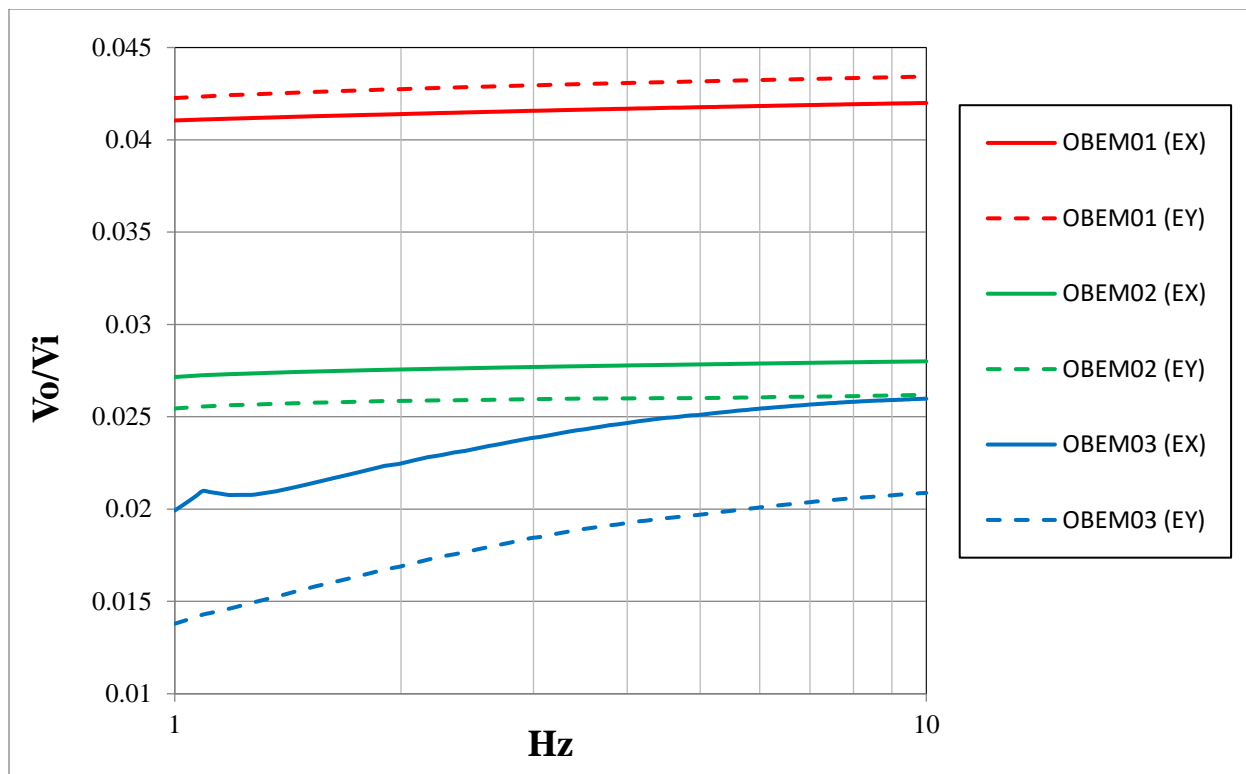


Figure 8

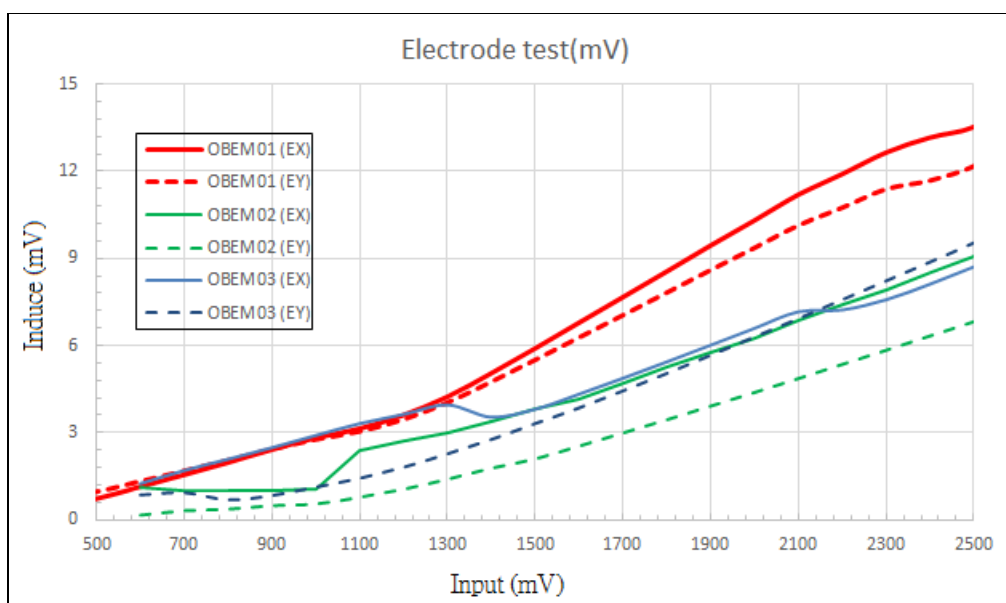


Figure 9



Figure 10



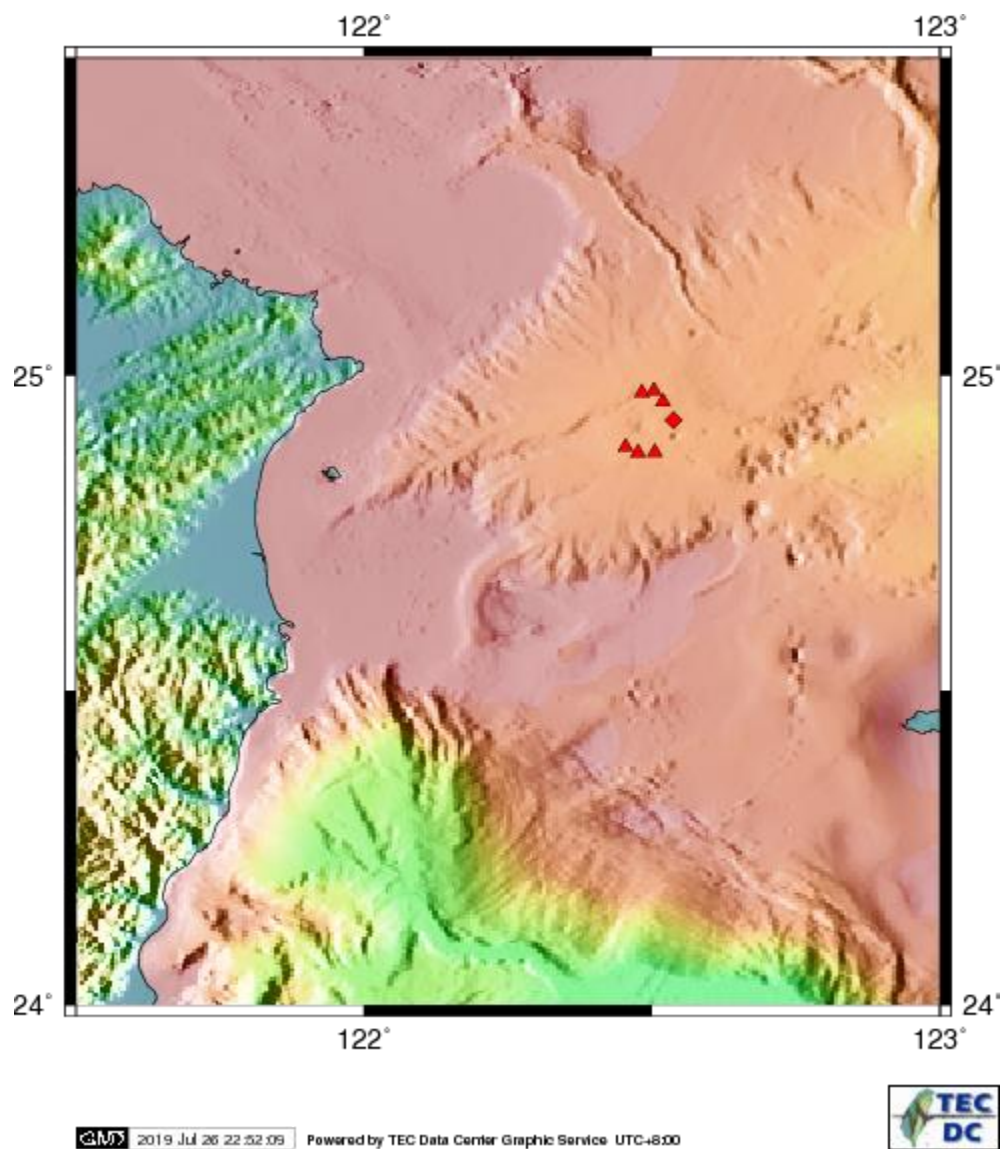


Figure 11

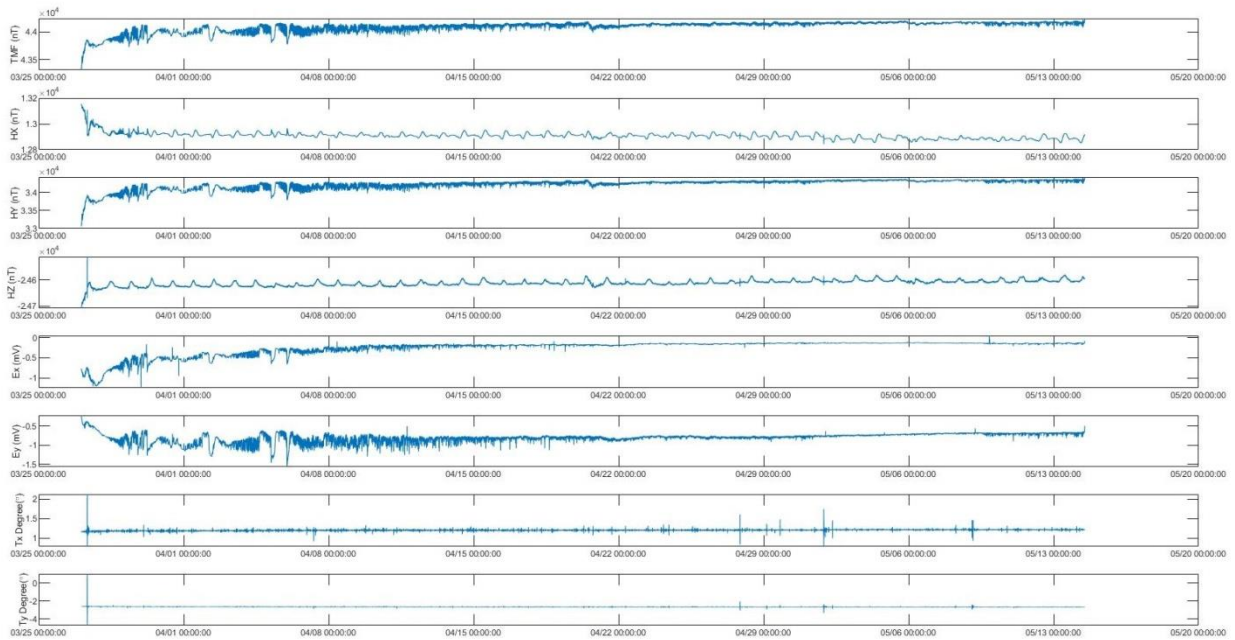


Figure 12

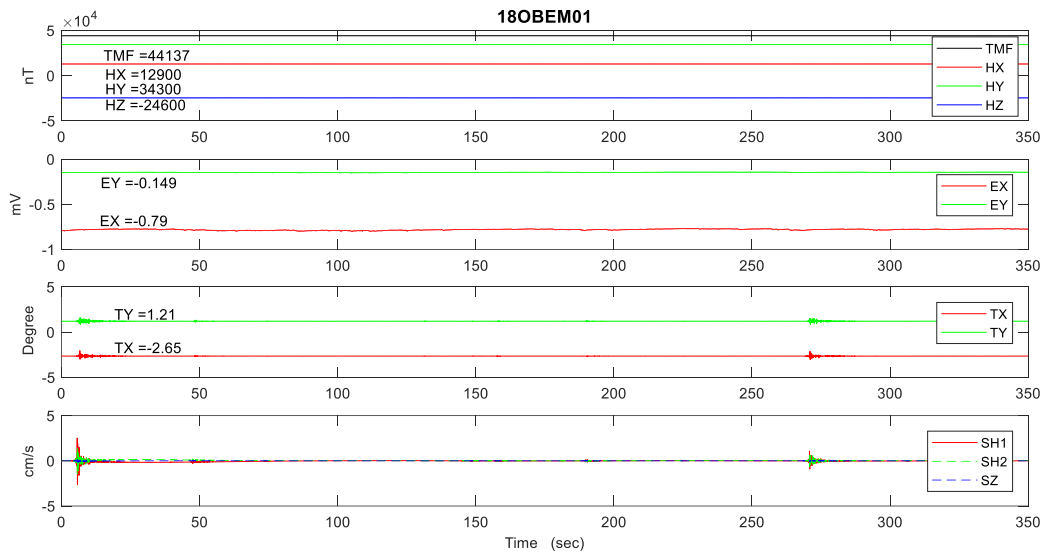


Figure 13

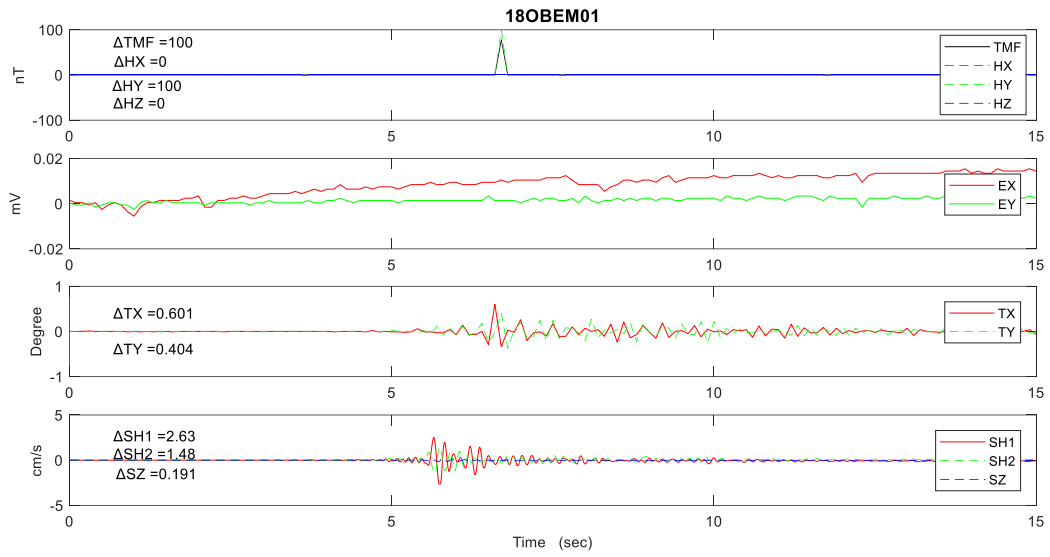


Figure 14